International Journal of Fracture (2005) 131:15–34
DOI 10.1007/s10704-004-1690-8

Application of instrumented indentation technique for enhanced fitness-for-service assessment of pipeline crack

JAE-IL JANG[1,5,*], YEOL CHOI[1], JUNG-SUK LEE[2], YUN-HEE LEE[2], DONGIL KWON[2], MING GAO[3] and RICHARD KANIA[4]
[1]*Frontics, Inc., Research Institute of Advanced Materials, Seoul National University, Seoul 151-742, Korea*
[2]*School of Materials Science and Engineering, Seoul National University, Seoul 151-742, Korea*
[3]*GE Power Systems Oil & Gas, 2702 North Loop West, Suite 6, Houston, TX 77008, USA*
[4]*GE Power Systems Oil & Gas, 1003-11th Street S. W., Calgary, Alberta, Canada T2R 1G2*
[5]*Current addresses: Department of Materials Science and Engineering, University of Tennessee, Knoxville, TN; Metals and Ceramics Division, Oak Ridge National Laboratory, Oak Ridge, TN, USA*
[*]*Author for correspondence (E-mails: jijang@frontics.com, jangj@ornl.gov)*

Received 15 December 2003; accepted in revised form 28 July 2004

Abstract. While most in-field non-destructive technologies for structural integrity diagnosis focus on precise crack detection, a novel instrumented indentation technique for non-destructively determining tensile properties in fields is introduced here. The goal of this work is to apply the newly-developed indentation technique to in-field fitness-for-service (FFS) assessment of linepipe cracks. As one step to verify its applicability, tensile properties in base metal and girth weldement of API-X65-graded linepipe were evaluated by this indentation technique and provided for construction of material-specific failure assessment diagrams (FADs). Results are discussed in terms of the accuracy of the indentation data and how the FAD assessment results are affected by the variation in local tensile properties measured by indenting small target regions such as heat-affected zones (HAZs). Based on the results, we suggest that the indentation technique may be useful for reducing possible difficulties in flaw assessment (arising from the use of incorrect tensile properties) by providing reliably practical data for FAD construction.

Key words: Failure assessment diagram (FAD), fitness-for-service (FFS), heat-affected zones (HAZ), instrumented indentation technique, pipeline crack, tensile properties, weld.

1. Introduction

The demand for accurate assessment of structural integrity has increased over the past decades to meet the increasing interest in safe and economical operation of industrial structures, and as a result many technologies and methodologies for flaw assessment have been developed. Nowadays, flaw assessment methods are generally performed based on a 'fitness-for-service (FFS)' concept using fracture mechanics rather than empirical inspections (Milne et al., 1988; Gordon, 1993; Denys, 1999; Anderson and Osage, 2000). Among these methods, the failure assessment diagram (FAD) is one of the most popular ways to assess crack-like flaws in industrial welded structures because it can predict not only brittle fracture but also plastic collapse (by which materials with sufficient toughness can fail). FAD methods are well presented

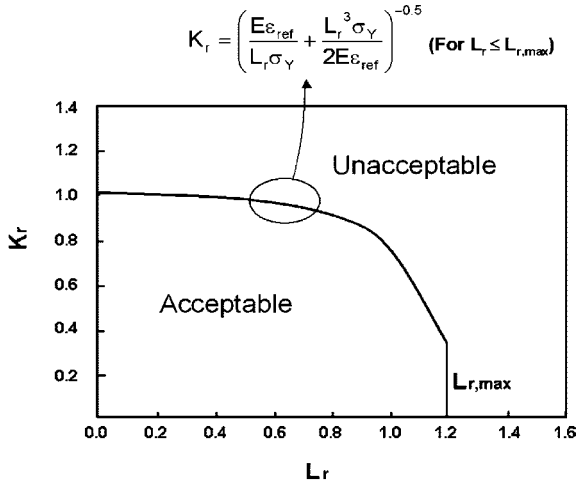

Figure 1. Typical material-specific failure assessment diagram (FAD) for a material.

in such current codes as R-6 (1998), BS 7910 (1999), SINTAP (1999) and API 579 (2000), all of which show various types of FADs.

The material-specific FAD, such as level 2B of BS7910, option 2 of R6, level 3B of API 579, and level 3 of SINTAP, is the least conservative FAD in situations where only representative material properties are given. Although every FAD code has higher-level FADs, such as option 3 of R6, they require a full J-integral analysis by finite-element methods, in addition to the material properties. Figure 1 shows a typical material-specific FAD (for a material without Lüders strain behavior) used in current codes for FFS assessment of crack-like flaws. The criterion line of material-specific FAD, the so-called failure assessment curve (FAC), is defined as in Equation (1), which requires the value of reference strain, ε_{ref}, of the target region including the flaws. Since ε_{ref} is defined as a corresponding true strain of the tensile curve at a true stress that is the same as the reference stress (σ_{ref}), the tensile curve of the target material must be determined before using the FAD:

$$K_r = \left(\frac{E\varepsilon_{ref}}{L_r\sigma_Y} + \frac{L_r^3\sigma_Y}{2E\varepsilon_{ref}} \right)^{-0.5}. \tag{1}$$

Here σ_Y and E are the yield stress and elastic modulus and L_r and K_r are the load and fracture ratios, respectively, as defined in Equations (2) and (3):

$$L_r = \frac{\sigma_{ref}}{\sigma_Y} \tag{2}$$

$$K_r = \frac{K_I}{K_{mat}} \tag{3}$$

where σ_{ref}, K_I and K_{mat} are reference stress, stress intensity factor, and fracture toughness, respectively. The reference stress (σ_{ref}), which can be determined by reference stress solution or limit load solution, is the effective stress applied on the ligament of flawed structure, and thus dependent on applied load and geometry of crack and structure. To determine the FAC and the point (L_r, K_r) indicating the crack's present status, material properties such as yield stress and fracture toughness

in Equations (2) and (3) are required. Additionally, the ultimate tensile stress is also required to define $L_{r,max}$, the limit value of plastic collapse, as in Equation (4):

$$L_{r,max} = \frac{\sigma_{flow}}{\sigma_Y} = \frac{(\sigma_Y + \sigma_U)/2}{\sigma_Y}, \tag{4}$$

where σ_{flow} and σ_U are flow stress and ultimate tensile stress, respectively.

As described above, the tensile properties (including true stress–true strain curve, yield and ultimate tensile strength) of the materials near the crack-like flaw are very important input parameters in assessing FFS according to current FAD codes. In most cases, however, conventional (standard) tensile tests, which may require specimens of a specific size and time-consuming procedures for specimen preparation and testing, cannot be used for in-field measurements without removing structural components. Additionally, evaluating the representative mechanical properties of welded joints, known to be among the weakest regions in any structure, has been always a headache for field engineers, since the joints have complex microstructural and mechanical gradients. For these reasons, direct evaluation of mechanical properties of in-service structural components, including welded joints, has been mainly limited to microhardness measurements. Although there have been many studies on converting hardness values to tensile strengths by empirical relationships, accurate true stress–true strain relationships cannot be obtained from conventional hardness tests.

With this in mind, here we suggest using an advanced indentation technique to provide reliably practical in-field tensile data of the target material for constructing a material-specific FAD. While most other in-field technologies related to structural reliability diagnosis focus merely on accurate crack detection, the advanced indentation technique, an instrumented indentation technique developed for industrial applications, can measure the stress–strain relationship and related material properties (such as yield strength, tensile strength, and work-hardening exponent) nondestructively by analyzing load–depth curve obtained during spherical indentation. This technique has many advantages to cope with present difficulties in obtaining in-field tensile properties useful for FAD construction: (i) the indentation system is portable and can thus be easily attached to components in service, (ii) properties of local regions like the heat-affected zone (HAZ) can be measured due to small indenter size (diameter 0.2–0.5 mm), (iii) the testing procedure is very simple and does not require time-consuming specimen preparation, (iv) no damage remains after testing. It thus has a strong potential to enhance the accuracy of life-time predictions and FFS assessments for industrial structures and facilities. In this paper, an application of the indentation technique to construction of material-specific FADs for assessment of pipeline cracks is introduced and discussed.

2. Advanced Indentation Technique

2.1. Analytical procedure

The advanced indentation technique, an instrumented indentation technique developed from the conventional hardness test, measures the indentation load and penetration depth during loading and unloading by a spherical indenter at constant speed (instead of the direct observation and measurement of indent size in a conventional

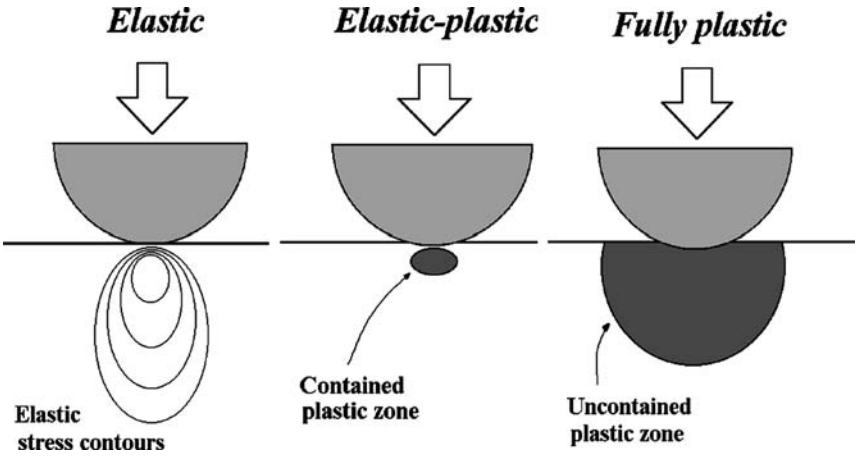

Figure 2. Schematic diagrams of three deformation stages during spherical indentation.

hardness test). The indentation load–depth curve obtained from this procedure is similar to the load–displacement curve from the uniaxial tensile test and represents the deformation behavior of the material beneath the rigid ball indenter. The true stress and true strain values, which are identical to the flow properties from the standard uniaxial tensile test, can be accurately predicted from analysis of indentation load–depth curve by considering the indentation stress fields and deformation shape.

During spherical indentation, mechanical deformation occurs in the three stages shown in Figure 2: elastic, elastic/plastic, and fully plastic (Francis, 1976). Reversible deformation occurs at low-load indentation. When the indentation stress fields satisfy the yield criterion, a plastic zone arises inside the material and expands to the free surface; the mean contact pressure beneath the spherical indenter increases rapidly in this elastic/plastic stage. Finally, the expanded hemispherical plastic zone grows into the surrounding elastic zone with constant velocity as the indentation depth increases; the mean contact pressure increases slightly in this fully plastic stage. This deformation stage is very close to the work-hardening behavior during an uniaxial tensile test. Thus, if the fully plastic stage during spherical indentation can be analyzed, the tensile properties, including the true stress–true strain curve, can be obtained according to the procedure described below.

Figure 3(a) shows a typical indentation load–depth curve for instrumented indentation tests. The representative stress and strain were defined in terms of measured indentation contact parameters such as contact depth (h_c), indenter shape and the morphology of the deformed sample surface. Real contact properties were determined by considering both elastic deflection and plastic material pile-up around the spherical indenter, as shown in Figure 3(b).

The contact depth at maximum indentation load can be evaluated by analyzing the unloading curve with the concept of indenter geometry and elastic deflection (Oliver and Pharr, 1992)

$$h_c^* = h_{\max} - \omega(h_{\max} - h_{\mathrm{i}}), \tag{5}$$

where h_{i} is the intercept indentation depth [see Figure 3(a)] and the indenter shape parameter ω is 0.75 for a spherical indenter. The material pile-up around the

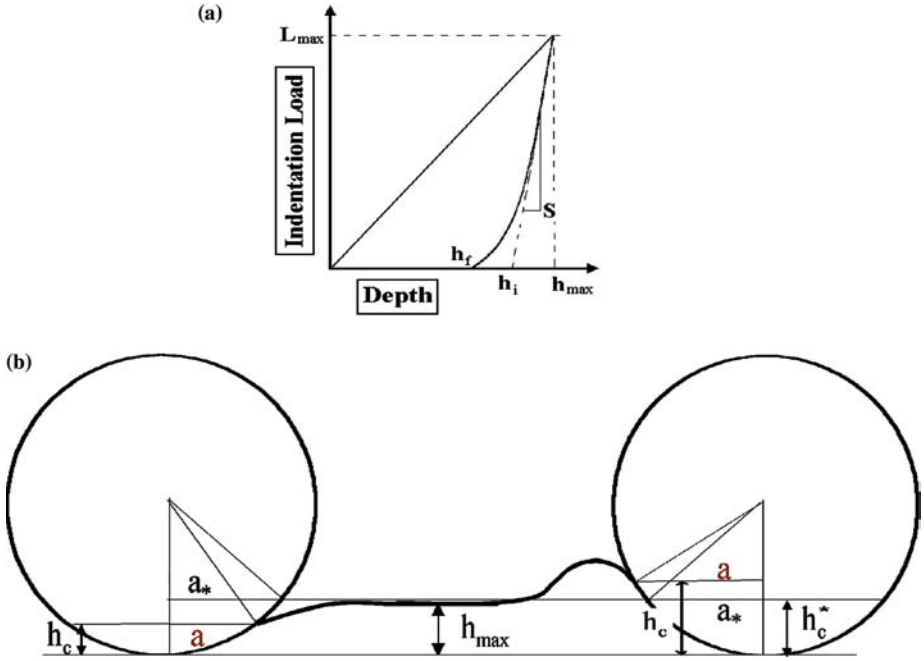

Figure 3. Schematic diagrams of (a) typical indentation load–depth curve (showing one loading–unloading sequence) and (b) elastic and plastic deformation around spherical indenter (left: sink-in, right: pile-up).

indentation makes the actual contact radius larger than expected. The extent of this pile-up can be expressed by a constant c and the steel work-hardening exponent n in Equation (6) (Norbury and Samuel, 1928; Hill et al., 1989)

$$c^2 = \frac{a^2}{a^{*2}} = \frac{5(2-n)}{2(4+n)}, \tag{6}$$

where a is the actual contact radius and a^* is the contact radius without the pile-up. From the geometry of the spherical indenter, the real contact radius is expressed in terms of h_c^* and indenter radius R as:

$$a^2 = \frac{5(2-n)}{2(4+n)}(2Rh_c^* - h_c^{*2}) \tag{7}$$

With these parameters, the representative stress and strain were determined as follows. The representative strain of indentation ε_R is evaluated from the material displacement beneath the indenter along the indentation axis direction. The strain can be expressed as in Equation (8) at the contact radius position by using a fitting constant α taken as 0.1 for various steels (Ahn and Kwon, 2001)

$$\varepsilon_R = \frac{\alpha}{\sqrt{1-(a/R)^2}}\frac{a}{R}. \tag{8}$$

Since the elastic and elastic/plastic deformation stages generally occur at very low indentation load in steels, only the plastic deformation stage is considered here. Using

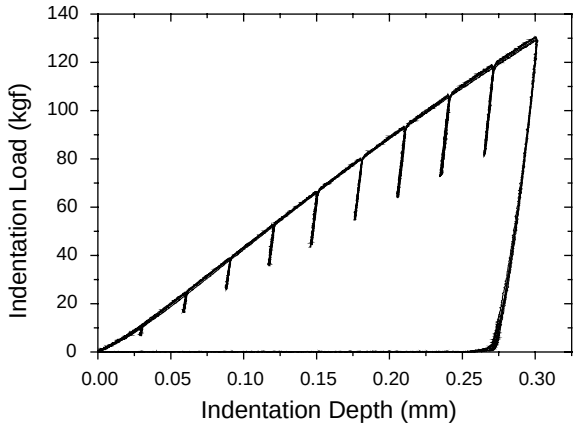

Figure 4. Typical load–depth curve obtained from instrumented indentation test with multiple loading–unloading sequences.

the mean contact pressure (P_{m}), obtained according to Equation (9) in terms of maximum load ($L_{\max}$) and contact area, the representative stress (σ_R) can be evaluated using the relationship with mean contact pressure in Equation (10) (Tabor, 1951):

$$P_{\mathrm{m}} = \frac{L_{\max}}{\pi \mathrm{a}^2} \tag{9}$$

$$\frac{P_{\mathrm{m}}}{\sigma_R} = \Psi, \tag{10}$$

where Ψ is a constraint factor for plastic deformation with upper limit about 3 for fully plastic deformation of steels (Tabor, 1951; Francis, 1976; Ahn and Kwon, 2001). When multiple loading–unloading sequences are made at one location on the target material, as shown in Figure 4, a series of representative stress and strain values is determined by analyzing each unloading curve according to the above procedure; then the values can be fitted as a simple power-law-type Hollomon equation (Dieter, 1988)

$$\sigma = K(\varepsilon)^n, \tag{11}$$

where K is the strength coefficient, and ε is total strain (should be equal to or larger than yield strain). The exact values of the work-hardening exponent and strength coefficient are calculated by the iteration method (Ahn and Kwon, 2001). While true stress always increases with true strain, the ultimate tensile strength can be determined using Consiére's criterion (Dieter, 1988) and the yield strength can be predicted through extrapolation of Equation (11) to the low-strain regime. The theoretical yield strain is usually described as the strain at the point where Equation (11) meets

$$\sigma = E\varepsilon \tag{12}$$

which is for linear elastic stress–strain regime, i.e., when strain ε is not larger than yield strain. However, since it is well accepted that Hollomon equation generally underestimates the stress values near the yield point (for example, see Kim et al.,

2001), the appropriate 0.2% offset yield strength was calculated in this indentation method by inputting strain value of 0.01 to Equation (11), as determined experimentally for structural steels (Jeon et al., 2003). The Young's modulus of steel was simply taken as 210 MPa in this study, as generally accepted, although it can be predicted by the instrumented indentation technique with some complex analysis (Oliver and Pharr, 1992).

2.2. Reliability verification

To appraise the reliability and reproducibility of the test results in the above procedure, tensile properties obtained from the advanced indentation tests were compared with those from uniaxial tensile tests. The comparisons were made in a blind test, and three representative metallic materials such as SS400 steel (low-strength steel), SCM4 steel (high-strength steel) and Al-2012 (non-ferrous metal) were tested. While the tensile properties of each material were measured twice in an uniaxial tensile tester, Instron 5582 (Instron Corp., Canton, MA, USA), the same target properties were measured four times by an instrumented indentation tester, AIS-2000 (Frontics, Inc., Seoul, Korea) using the above procedure. Figures 5 and 6 show the results of each test. All samples show good repeatability of the true stress–true strain curves from tensile tests (Figure 5) and true stress–true strain curves converted from indentation load–depth curves (Figure 6). The tensile properties measured by indentation tests were compared with those from uniaxial tensile tests in Table 1; this comparison shows that the advanced indentation tests can provide tensile properties nondestructively.

3. Experimental Procedure

Commercial API-5L-X65-graded pipelines of outer diameter 762 mm and thickness 17.5 mm, which are generally used in Korea as natural gas transmission pipelines, were studied. The API X-65 steels, whose chemical composition and carbon equivalent are listed in Table 2, are manufactured by a thermomechanical-controlled-process (TMCP) and have low carbon equivalent for good HAZ toughness and weldability. To make girth weldments, the ends of each pipe were machined into a V-groove configuration and welded by gas tungsten arc welding (GTAW) and shielded metal arc welding (SMAW) under the same welding conditions as used for actual girth welding of natural gas pipeline in Korea.

For FFS assessment of virtual flaws, advanced indentation tests were made on various locations of girth-welded pipe; the locations were selected arbitrarily from girth welds and base metal. A portable instrumented indentation system, AIS-2000 (Frontics, Inc., Seoul, Korea) was used to measure the tensile properties by the advanced indentation technique. After the target regions were polished by a hand grinder, the indentation system was attached to the outer pipe surface by curved magnets. Although the tests here were made in the laboratory, all the testing procedures, including the attachment method, were those used for on-site tests in order to simulate the poor testing environment in the field. The photographs in Figure 7 of in-field pipeline indentation tests show the measurement of the pipeline tensile

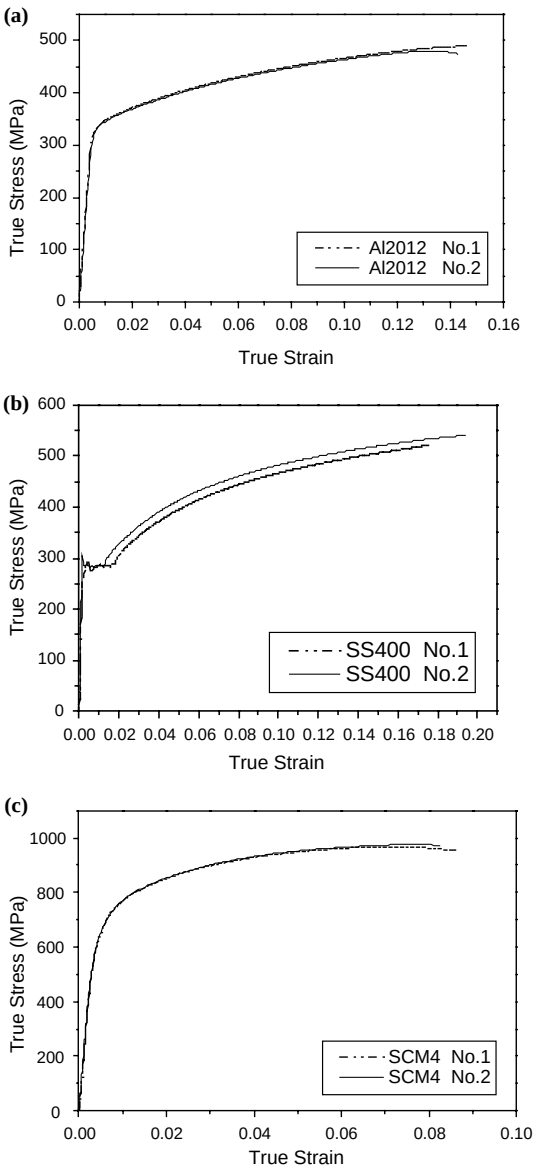

Figure 5. True stress versus true strain curves obtained from uniaxial tensile tests: (a) Al2012, (b) SS400, and (c) SCM4.

properties by attaching the indentation system to the outer surface. The indentation system in the photos is the same as that used in this study.

The radius of the spherical indenter used in this study was 250 μm, and multiple loading–unloading sequences were made at 0.3 mm/min. During indentation, load–displacement curves were continuously obtained and converted to true stress–true strain curves.

To verify the accuracy of the data obtained, some parts of the base materials, including the indented regions, were removed from the pipe and machined for uniaxial tensile tests, all of which were performed according to ASTM E8 (1991). For

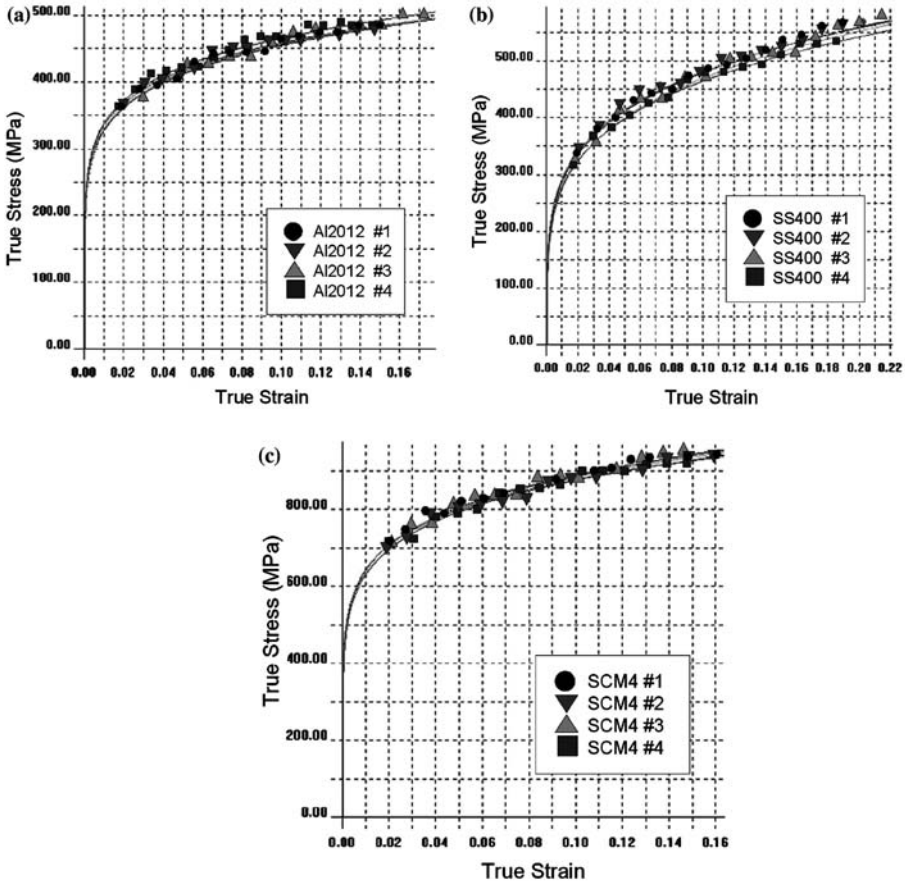

Figure 6. Superposition of true stress–true strain curves converted from indentation load–depth curve: (a) Al2012, (b) SS400, and (c) SCM4.

welds that included HAZs, uniaxial tests were not done because the abrupt changes in microstructure and mechanical properties within the narrow weld area make it very difficult to prepare a standard-sized specimen and to obtain representative values for comparison with tensile values of local areas from indentation tests.

4. Results and Discussions

4.1. Assessment of cracks in base metal

Advanced indentation tests were carried out at positions selected arbitrarily within the base-metal part of the girth-welded pipe. Figure 8 superposes multiple indentation load–depth curves and the true stress–true strain curves obtained from the advanced indentation tests. Although these results are from just the base-metal part of one pipe unit, it can be seen there are variations in flow curves, possibly arising during manufacture like steel-making and pipe-forming process. It should be noted that Lüders strain, generally observed in API steel, is not shown in Figure 8(b) because it cannot be predicted by our procedure, as discussed below.

Table 1. Comparison of results from advanced indentation tests with those from uniaxial tensile tests.

Materials	Testing methods	Yield strength (MPa)	Tensile strength (MPa)	Work-hardening Exponent
Al2012	Indentation tests			
	No. 1	327.2	479.4	0.143
	No. 2	335.3	478.5	0.136
	No. 3	329.6	480.8	0.142
	No. 4	338.0	487.9	0.139
	Average (I)	332.5	481.6	0.140
	Tensile tests			
	No. 1	334.9	489.2	0.137
	No. 2	332.1	480.3	0.136
	Average (T)	333.5	484.8	0.137
	Difference between I and T (%)	0.3	0.6	2.7
SS400	Indentation tests			
	No. 1	288.6	572.1	0.221
	No. 2	293.5	566.6	0.215
	No. 3	275.6	571.7	0.232
	No. 4	278.8	555.3	0.222
	Average (I)	284.1	566.4	0.222
	Tensile tests			
	No. 1	282.4	520.7	0.237
	No. 2	285.8	540.0	0.219
	Average (T)	284.1	530.4	0.228
	Difference between I and T (%)	0.0	6.8	2.4
SCM4	Indentation tests			
	No. 1	642.7	933.4	0.141
	No. 2	644.8	913.0	0.134
	No. 3	645.7	924.2	0.137
	No. 4	632.0	921.2	0.142
	Average (I)	641.3	923.0	0.139
	Tensile tests			
	No. 1	681.0	968.0	0.129
	No. 2	687.2	975.2	0.131
	Average (T)	684.1	971.6	0.130
	Difference between I and T (%)	6.3	5.0	6.6

To assess the reliability of the advanced indentation test by comparing its data with uniaxial tensile test data, two arbitrary locations A and B were selected within the base metal. Material near A and B was cut off from the pipe and machined into dog-bone-shaped standard tensile specimens (gauge length 25 mm, width 6 mm, and

Table 2. Chemical composition and carbon equivalent (Ceq) of API 5L X65 pipeline steel.

Element	C	P	Mn	S	Si	Fe	$C_{eq.}$
Composition (wt%)	0.08	0.019	1.45	0.003	0.31	Bal.	0.32

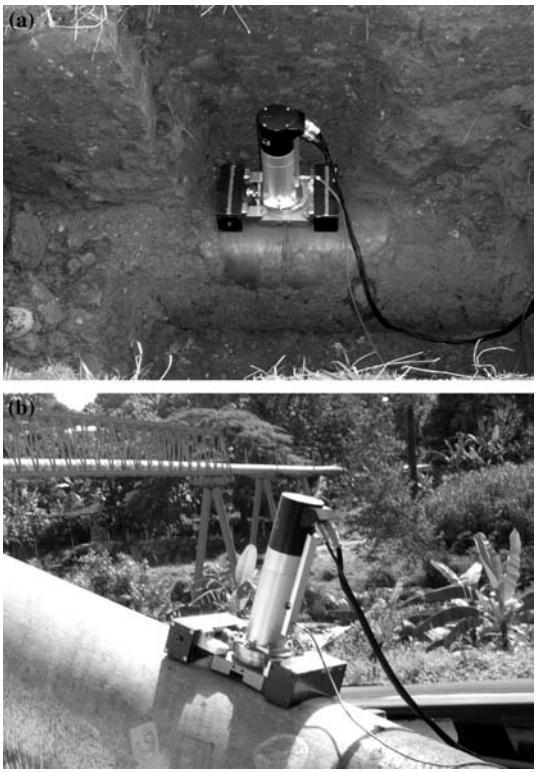

Figure 7. In-field indentation tests: instrumented indentation system attached to (a) underground pipeline, and (b) aboveground pipeline.

thickness 4 mm). True stress–true strain curves from advanced indentation tests are compared with those from uniaxial tensile tests in Figure 9. While the flow curves from both tests show very good agreement for the fully plastic regions, they differ in the Lüders strain observed in uniaxial tensile tests. As a material-specific FAC shape is dependent upon the presence of the Lüders strain and its length, inability to evaluate Lüders strain may bring a serious difficulty in an application of the indentation technique to FAD construction. Although many indentation studies have suggested that the unstable yielding phenomena can be predicted by analyzing the relationship between material pile-up around the spherical indenter and the work-hardening exponent (for example, see Choi et al., 2001), the procedure suggested requires *ex-situ* observation of pile-up height with appropriate microscopy, which would make in-field testing more complex and, in many cases, impossible. To maximize in-field applicability of the new testing technique, non-destructive Lüders strain measurement by microscopy was not considered in our indentation testing procedure. Therefore, the awareness of Lüders strain existence (or absence) is essentially

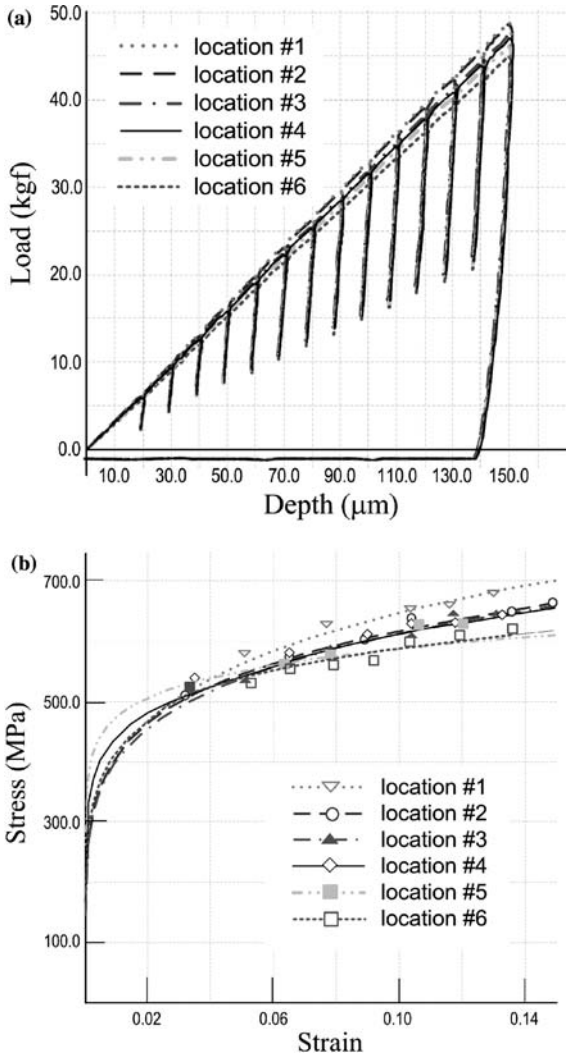

Figure 8. Superposition of various (a) load–depth curves and (b) converted true stress–true strain curves obtained from advanced indentation tests on base-metal part of pipe.

needed before the indentation technique is applied to FAD construction. Hopefully, in most cases of structural steels, this issue may be simply solved by checking the type of target material. In this study, because API X65 linepipe steel is well known to have the unstable yielding phenomena, the existence of Lüders strain was assumed in the strain range below 0.02 for all samples during constructing FAD. Based on this assumption, the yield strengths from the indentation tests were determined by putting $\varepsilon = 0.02$ into Equation (11). Table 3 summarizes the values of the tensile properties (yield strength, tensile strength, and work-hardening exponent) obtained from both indentation and tensile tests. It is seen that the results from the indentation tests shows good agreement with those from uniaxial tensile test results.

A material-specific FAD was constructed and FFS assessment for possible cracks was simulated using the base-metal tensile properties obtained from the advanced indentation tests. Figure 10 shows schematic diagrams of the pipe and a virtual crack

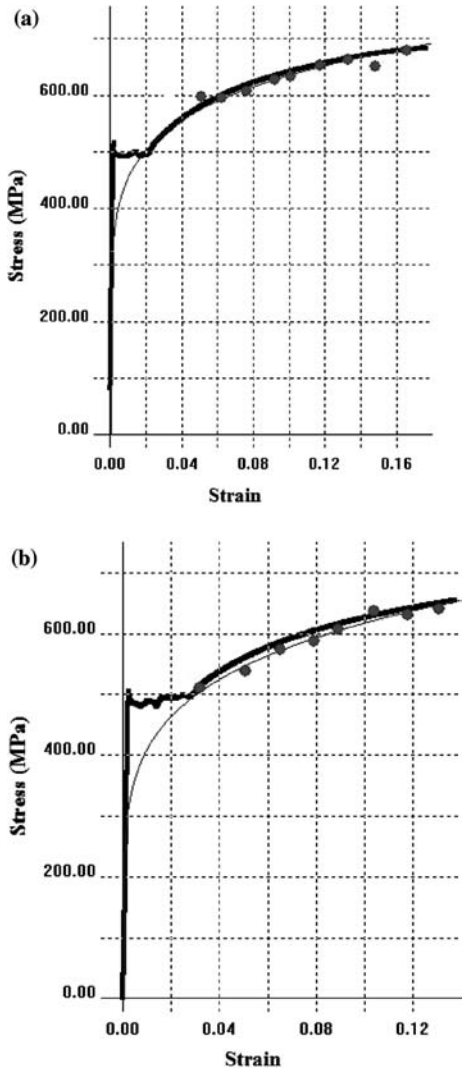

Figure 9. Comparison of flow curves obtained from advanced indentation tests with those from uniaxial tensile tests: (a) location A and (b) location B (bold line is from uniaxial tests; lighter line and spot are from indentation tests).

Table 3. Tensile properties obtained from advanced indentation tests and from uniaxial tensile tests.

Location	Properties	Uniaxial tensile test	Advanced indentation test
A	YS (MPa)	488	487
	UTS (MPa)	674	673
	Work-hardening Exponent	0.143	0.153
B	YS (MPa)	485	469
	UTS (MPa)	654	656
	Work-hardening Exponent	0.163	0.162

Based on the assumption of Lüders strain existence, the yield strengths from the indentation tests were determined by putting $\varepsilon = 0.02$ into Equation (11).

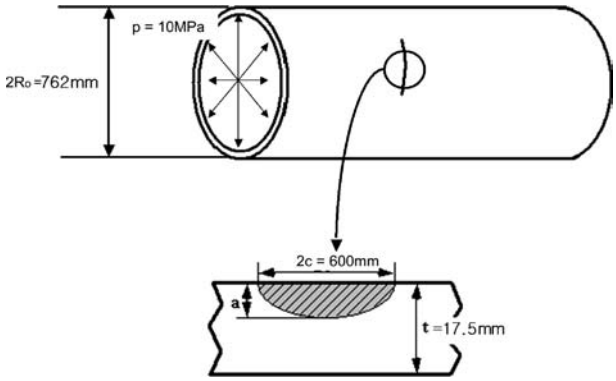

Figure 10. Schematic diagram of pipe geometry and virtual crack condition.

condition. A circumferential crack is assumed to exist in the base-metal part of the pipe (thickness 17.5 mm, outer diameter 762 mm). Only internal pressure was assumed as an applied force; the pressure used is 10 MPa, a little bit above the 7 MPa general operating pressure of natural gas pipeline in Korea. The crack length was fixed as 600 mm and crack depth was varied. The reference stress for the given condition was obtained according to the following reference stress solution in API579 (2000):

$$\sigma_{\text{ref}} = \left[\frac{2\arccos\left(A\sin\theta\right)}{\pi} - \frac{x\theta}{\pi}\left(\frac{2-2\tau+x\tau}{2-\tau}\right)\right]^{-1}\left(\frac{\mathrm{p}R_{\text{i}}^2}{R_o^2-R_{\text{i}}^2}\right)$$
$$\text{where } A = x\left[\frac{(1-\tau)(2-2\tau+x\tau)+(1-\tau+x\tau)^2}{2\{1+(2-\tau)(1-\tau)\}}\right],$$
$$\tau = \frac{t}{R_{\text{o}}}, \quad x = \frac{a}{t}, \quad \theta = \frac{\pi c}{4R_{\text{o}}}. \tag{13}$$

The p, R_{o} and R_{i} are internal pressure, outer radius and internal radius of pipe, respectively, and a, c, and t are as schematically shown in Figure 10.

To construct a FAD, fracture toughness values are also essential. Since fracture toughness cannot be assessed in the indentation test itself, crack-tip-opening displacement (CTOD) values from previous research (Lee et al., 2002) were used. The CTOD values converted into K_{IC} values using Equation (14) (of the various equations converting CTOD to K_{IC} in current FAD codes, this equation is the least conservative for API X65-grade pipeline):

$$K_{\text{IC}} = \sqrt{\frac{2\sigma_{\text{Y}} E\delta_{\text{IC}}}{1-\nu^2}} \tag{14}$$

where δ_{IC} is the critical CTOD value and ν is Poisson's ratio. Although some research have been done on indentation techniques for measuring fracture toughness non-destructively (for example, see Byun et al., 1998), most attempts have been unsuccessful because they require important material properties such as fracture strength to be known before testing.

The tensile values at locations A and B were input to assess the crack mentioned above. Figure 11 shows the results of FFS assessment using FAD. Although

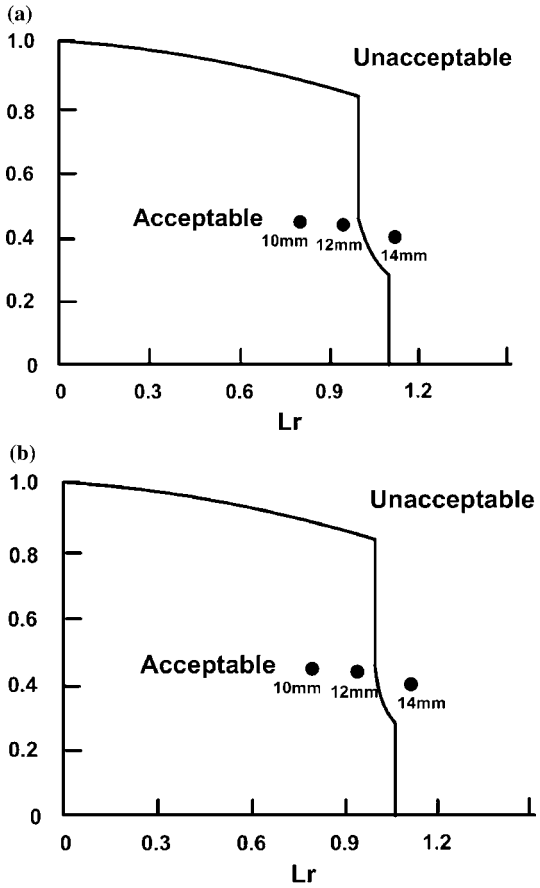

Figure 11. Results of FFS assessment for the virtual crack (in Figure 10) according to change in crack depth: (a) location A and (b) location B.

the locations have different flow properties (see Table 3 and Figure 9), both assessment results show almost identical failure conditions except for a slight difference in $L_{\max}$. However, this result does not mean that advanced indentation technique cannot enhance the accuracy of FFS assessment. It should be noted that the pipe used in this study was new and had not experienced the degradation from aging and environmental effects found in in-service pipe, especially buried pipelines and those exposed to high temperatures. Materials degraded by long-term operation have mechanical properties, including flow curve, different from those of new materials because of softening (or hardening), embrittlement, and the like. In such cases, using new-material tensile properties in FAD construction can cause incorrect assessment of crack acceptability. This incorrect assessment, which may lead with continued operation to a dangerous situation, can be prevented by measuring the reliably practical tensile properties using the advanced indentation technique. Thus, if proper tensile data from the advanced indentation technique are used in FAD construction, the accuracy of the FFS assessment results will surely be enhanced. In addition, the above results suggest that the indentation location can be selected arbitrarily within the base-metal when a crack is located at a base-metal region; it is not necessary to evaluate the location closest to the crack.

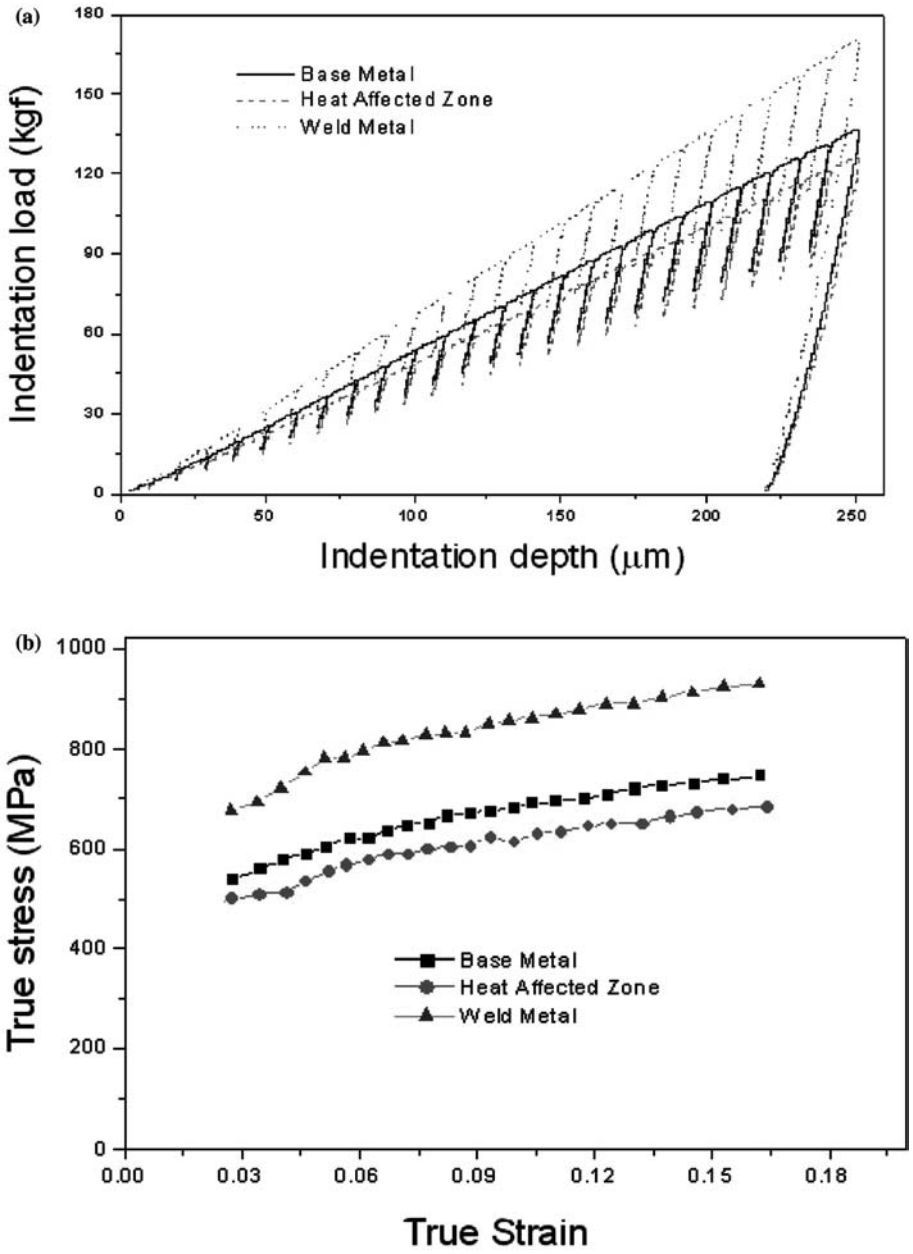

Figure 12. Variations in (a) indentation load–depth curve and (b) flow properties with the change in testing locations.

4.2. Assessment of cracks in welds

It is generally accepted that welding can significantly degrade the microstructural and mechanical properties of materials; thus cracking susceptibility is much higher in weldments than in the base metal. If a crack exists within welds, however, FFS assessment using current FAD codes is more difficult because the mechanical properties of welds are difficult to measure by conventional mechanical tests such as

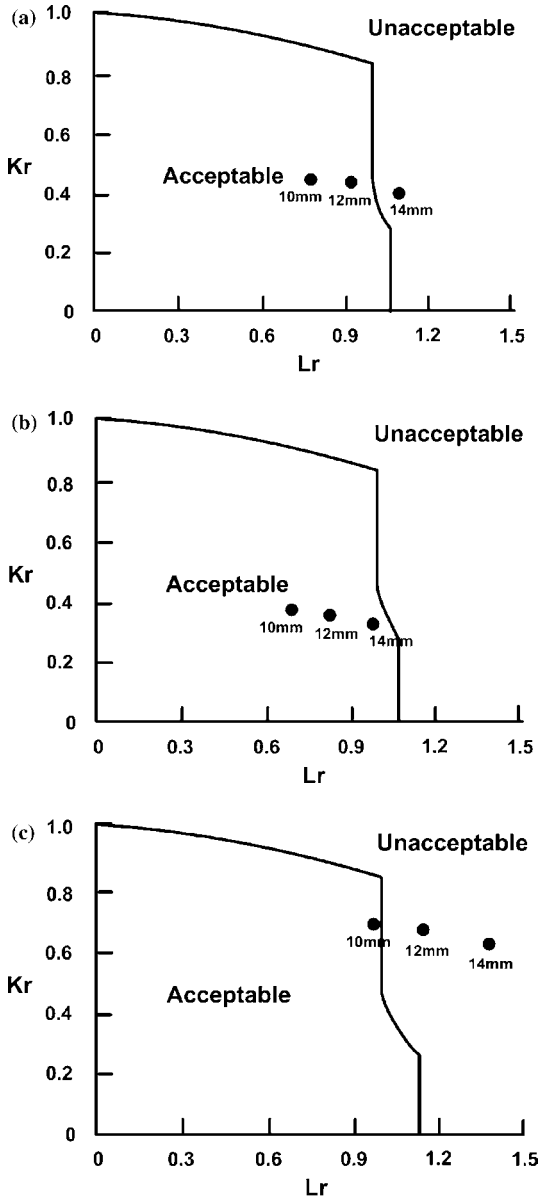

Figure 13. Results of FFS assessment for virtual crack located in (a) base metal, (b) weld metal, and (c) HAZ, according to change in crack depth.

uniaxial tensile tests. In particular, it is significantly more difficult to evaluate HAZ tensile properties than those of base metal and weld metal due to the complex microstructural gradients in HAZs; in addition, HAZs are so narrow that specimens for mechanical property measurements are difficult to be produced. For these reasons, current codes usually recommend using either weld-metal properties (for undermatched joint) or base-metal properties (for overmatched joint) instead of HAZ properties when flaws exist in the HAZ. Also, using the equivalent properties between weld and base-metal properties is suggested for HAZ flaws in SINTAP (1999), and the use of weld-metal properties is recommended for flaws in regions twice the width of the weld metal

in API 579 (2000). These difficulties in selecting appropriate mechanical properties for HAZ, too, can be solved by using the advanced indentation technique, which can evaluate the tensile properties of very local regions like HAZ.

In this study, advanced indentation tests were performed across welded joints and the FADs for weld metal, HAZ, and base metal were constructed using tensile data from the indentation tests. Figure 12 shows multiple indentation load–depth curves and true stress–strain curves from indentation tests for three regions. The weld metal has the highest strength and the HAZ has lowest strength of the three regions. Since yield stress generally indicates resistance to plastic collapse, the HAZ of this steel is more susceptible to plastic collapse than the weld metal and even the base metal. The poor HAZ properties are due to the softening behavior of API steel. Generally, HAZs of TMCP steels such as the API X65 steel in this study soften during welding due to decomposition of the strengthened martensitic (or bainitic) matrix by overtempering: the high-temperature welding processes alter the hard low-temperature transformation products to the soft high-temperature products (Mohandas et al., 1999; Ju et al., 2002).

For the flaw conditions described in Figure 10, the material-specific FADs for these three regions were constructed using the tensile properties of each part. As in the base-metal case discussed above, crack length was fixed at 600 mm and only the crack depth was variable. The input values of K_{IC} were 268 MPa(m)$^{1/2}$ for weld metal, 300 MPa(m)$^{1/2}$ for base metal, and 153 MPa(m)$^{1/2}$ for HAZ, which were converted from CTOD values obtained previously (Lee et al., 2002) with Equation (14). Figure 13 shows the results of crack assessment by the FADs constructed using indentation-test tensile properties. The three FADs show totally different failure assessment boundary conditions. In the HAZ-specific FAD, even a 12-mm-deep crack is not acceptable, while a 14-mm-crack is acceptable in weld metal. These results show how, if a crack is located at the welded joints, the FFS assessment results can differ widely according to tensile properties of the material. Additionally, the above results mean that, when a crack is present in the HAZ, the use of either weld metal or base metal properties instead of HAZ properties (as in current codes) can produce a wrong assessment result; i.e., a dangerous situation can be assessed as a safe situation. These inaccuracies are remedied by conducting advanced indentation tests near the crack and using the tensile data thus obtained to assess the crack condition with FAD.

5. Concluding Remarks

This work suggests that the advanced indentation technique may be useful for reducing possible difficulties in flaw assessment (arising from the use of incorrect tensile properties) by non-destructively providing practical tensile properties of the target structures/components in fields. Although there can be additional mechanical factors considerable for more critical crack assessment of welded structures, such as welding residual stress and constraint/tri-axial effects (due to strength mismatch and geometry/thickness), it is hoped that this study will be valuable in providing a new direction for in-field evaluation of structural integrity, especially in the pipeline industry. Additionally, it is interesting to consider that, some effort is currently being devoted to developing another instrumented indentation technique to measure welding residual stress (Jang et al., 2003), also an important factor in FFS assessment of welded structures. If this technique is established and combined with the advanced indentation

technique introduced in this paper, one may expect that the accuracy of in-field FFS assessment can be significantly enhanced.

Acknowledgements

This work was performed as cooperative research among Frontics, Inc., GE Power Systems, Inc. and Seoul National University. The authors at Seoul National University (J.S. Lee and D. Kwon) wish to thank the Korean Ministry of Science and Technology for providing financial support for this work under the National Research Laboratory (NRL) Program.

References

Ahn, J.-H. and Kwon, D. (2001). Derivation of plastic stress–strain relationship from ball indentation: Examination of strain definition and pileup effect. *Journal of Materials Research* **16**, 3170–3178.

Anderson, T.L. and Osage, D.A. (2000). API 579: A comprehensive fitness-for-service guide. *International Journal of Pressure Vesssels and Piping* **77**, 953–963.

API 579 (2000). *Recommended Practice for Fitness for Service*, American Petroleum Institute, Washington, DC.

ASTM E8–91 (1991). *Standard Test Methods of Tension Testing of Metallic Materials*, American Society for Testing and Materials, Philadelphia, PA.

BS 7910 (1999). *Guide and Methods for Assessing the Acceptability of Flaws in Fusion Welded Structures*, British Standards Institution, London, UK.

Byun, T.S., Kim, J.W. and Hong, J.H. (1998). A theoretical model for determination of fracture toughness of reactor pressure vessel steels in the transition region from automated ball indentation test. *Journal of Nuclear Materials* **252**, 187–194.

Choi, Y., Ahn, J.-H., Choi, J.K., Choo, W.Y. and Kwon, D. (2001). Evaluation of Lüders strain by analyzing the deformation characteristics around the residual indentation in structural steel. *Journal of the Korean Institute of Metals and Materials* **39**, 50–58.

Denys, R.M. (1999). Girth-weld defect qualification methods need to be rationalized. *Pipe Line & Gas Industry* **82–89**, 35–41.

Dieter, G.E. (1988). *Mechanical Metallurgy*, McGraw-Hill, London, UK, pp. 283–292.

Francis, F.A. (1976). Phenomenological analysis of plastic spherical indentation. *Journal of Enginnering Materials and Technology–Transaction of the ASME* **98**, 272–281.

Gordon, J.R. (1993). A review of fracture assessment procedures and their applicability to welded structures. *Canadian Metallurgical Quarterly* **32–33**, 195–203.

Hill, R., Storåkers, B. and Zdunek, A.B. (1989). A theoretical study of the Brinell hardness test. *Proceedings of the Royal Society of London* **A423**, 301–330.

Jang, J.-i., Son, D., Lee, Y.-H., Choi, Y. and Kwon, D. (2003). Assessing welding residual stress of A335 P12 steel welds before and after stress-relaxation annealing thorough instrumented indentation technique. *Scripta Materialia* **48**, 743–748.

Jeon, E.-C., Park, J.-S. and Kwon, D. (2003). Statistical analysis of experimental parameters in continuous indentation tests using Taguchi method. *Journal of Engineering Materials and Technology–Transaction of the ASME* **125**, 406–411.

Ju, J.-B., Lee, J.-S., Jang, J.-i., Kim, W.-S. and Kwon, D. (2002). Metallurgical and mechanical features of API 5L X65 pipeline steel weldment. *Proceedings ofthe 4th International Pipeline Conferences-IPC2002*, Paper No. IPC02–27180 (Published on CD-ROM).

Kim, S.K., Kim, Y.M., Lim, Y.J. and Kim, N.J. (2001). *Proceeding of the 15th Conference on Mechanical Behavior of Materials*, Korean Institute of Metals and Materials, Korea, pp. 177–186.

Lee, J.-S., Ju, J.-B., Jang, J.-i., Kim, W.-S., Kho, Y.-T. and Kwon, D. (2002). Fitness-for-service assessment for crack-like flaws of the welded structure using failure assessment diagram. *Journal of the Korean Institute of Metals and Materials* **40**, 1034–1041.

Milne, I., Ainsworth, R.A., Dowling, A.R. and Stewart, A.T. (1988). Background and validation of CEGB report R/H/R-6 revision 3. *Internationl Journal of Pressure Vessels and Piping* **32**, 105–196.

Mohandas, T., Madhusudan, R.G. and Satish, K.B. (1999). Heat-affected zone softening in high-strength low-alloy steels. *Journal of Materials Processing Technology*. **88**, 284–294.

Norbury, A.L. and Samuel, T. (1928). The recovery and sinking-in or piling-up of material in the Brinell test, and the effects of these factors on the correlation of the Brinell with certain other hardness tests. *Journal of Iron & Steel Institute* **117**, 673–687.

Oliver, W.C. and Pharr, G..M. (1992). An improved technique for determining hardness and elastic modulus using load and displacement sensing indentation experiment. *Journal of Materials Research* **7**, 1564–1583.

R-6: (1998). Assessment of the integrity of structures containing defects, British Energy, R/H/R-6-Revision 3.

SINTAP (1999). Structural Integrity Assessment Procedures for European Industries, Final Procedure, European Union Brite-Euram Programme, Project Number BE95-1426.

Tabor, D. (1951), *The Hardness of Metals*, Oxford Univ Press, Oxford, UK, pp. 79–83.